Available online at www.sciencedirect.com

SciVerse ScienceDirect

Procedia Engineering 00 (2016) 000–000

Procedia Engineering

www.elsevier.com/locate/procedia

25th International Meshing Roundtable (IMR25)

An Anisoptropic Surface Remeshing Strategy Combining Higher Dimensional Embedding with Radial Basis Functions

Franco Dassi, Patricio Farrell, Hang Si

Weierstrass Institute for Applied Analysis and Stochastics, Mohrenstr. 39, 10117 Berlin, Germany

Abstract

Many applications heavily rely on piecewise triangular meshes to describe complex surface geometries. High-quality meshes significantly improve numerical simulations. In practice, however, one often has to deal with several challenges. Some regions in the initial mesh may be overrefined, others too coarse. Additionally, the triangles may be too thin or not properly oriented. We present a novel mesh adaptation procedure which greatly improves the problematic input mesh and overcomes all of these drawbacks. By coupling surface reconstruction via radial basis functions with the higher dimensional embedding surface remeshing technique, we can automatically generate anisotropic meshes. Moreover, we are not only able to fill or coarsen certain mesh regions but also align the triangles according to the curvature of the reconstructed surface. This yields an acceptable trade-off between computational complexity and accuracy.

Peer-review under responsibility of organizing committee of the 25th International Meshing Roundtable (IMR25).

1. Introduction

Countless numerical methods need to transfer information from a continuous domain to discrete points on a grid. Most commonly this problem arises when solving partial differential equations numerically but it also appears in the context of surface approximation [8,14,16,22] or medical image reconstruction [11].

Finding *optimal* grids is of uttermost importance. Obviously, optimal can mean many things. However, two desirable features stand out. On the one hand, our grid should be built in such way that the data we are interested in (for instance the solution of a partial differential equation) is approximated fairly accurate. That is, we want to grasp finer details (for example along boundary layers) as well as large-scale variations. On the other hand, we want to be able to efficiently compute the discrete approximation and only use nodes which enhance its quality.

This leads naturally in 2D and 3D to anisotropic grids which are able to achieve a reasonable trade-off between accuracy and efficiency. Anisotropic grids are often used in the context of finite element and finite volume methods and thus appear very frequently in practical applications [12,13,15]. However, how to obtain such an anisotropic mesh for a given application is an open problem. Unfortunately, not many numerical analysts focus on the art of designing precise grids but rather on discretization techniques for the solution of partial differential equations.

E-mail addresses: dassi@wias-berlin.de (Franco Dassi)., patricio.farrell@wias-berlin.de (Patricio Farrell)., si@wias-berlin.de (Hang Si).

Peer-review under responsibility of organizing committee of the 25th International Meshing Roundtable (IMR25).

In this paper, we study how to automatically obtain curvature-adapted surface meshes from low-quality ones. We explicity point out that curvature-adapted surface meshes may not be necessarily useful in the context of differential equations (as the curvature may not be a reasonable indicator for where a refinement of the computational domain is needed). However, curvature-adaptation makes visualizing complex data sets more efficient. The initial low-quality mesh may be too coarse in certain regions or too dense in others. Also, in practice one has to deal with improperly oriented triangles. While a strechted triangle is not per se unacceptable, it should not be stretched in the direction of maximum curvature. Figure 1 shows what our method is capable of. The original mesh on the left is extremely coarse and uniform. The adapted mesh, on the other hand, is denser and refined where necessary. The stretched triangles reflect nicely the curvature. For example, the curvature along the dashed arrows varies more than along the corresponding solid ones. Hence, we need to refine more in the direction of the dashed arrows which means that the triangles will be stretched along the solid arrows.

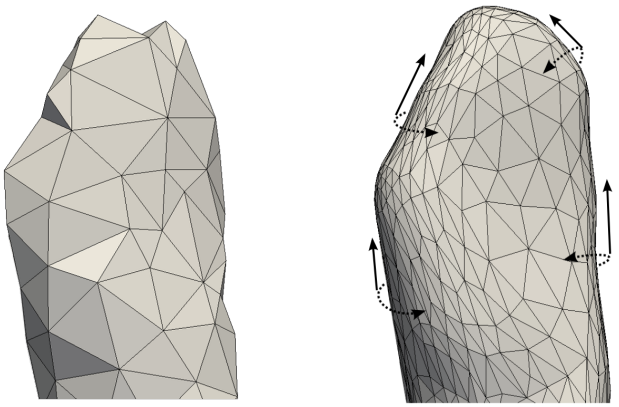

Fig. 1: A coarse input mesh on the left and the adapted mesh using the novel adaptation procedure on the right.

The key idea of our method is to combine surface approximation by radial basis functions with the higher dimensional embedding technique. Radial basis functions (RBFs) have been used for decades in the context of multivariate data approximation [9,10,18,24]. Ironically, their main selling point is that they can be used to interpolate unstructured data without relying on a mesh. Even though they are most commonly used in the context of *meshfree* data approximation, they sometimes have been employed in the context of mesh repair. Carr et al. [2] used polyharmonic radial basis functions to fill in incomplete meshes. Similarly, Marchandise et al. [20] developed a method to repair meshes obtained from a CAD model or an STL triangulation [5].

The higher dimensional embedding (HDE) was introduced by Cañas et al. in [1]. Since then several authors have expanded their ideas [4,6,19]. HDE produces an anisotropic triangular curvature-adapted surface mesh that fits an input surface. The anisotropy is obtained by finding a higher-dimensional space in which the mesh is assumed to be uniform and isotropic. Previously other approaches based on metric tensor fields [14,16] or minimizing objective functionals [8,22] have been studied. However, in order to be able to apply both of these strategies one needs to have a priori or a posteriori knowledge of the error, which depends on the problem itself. The HDE, on the other hand, does not require any information on the error. It is solely based on information provided by the embedding map. Note, in [4] the original geometry is given via a known CAD model. In this paper, however, we will additionally reconstruct the original geometry. Hence the only input needed is an initial mesh which might have some of the previously described issues.

This paper is organized as follows. After introducing the higher dimensional embedding technique and radial basis functions in the second and third sections, we present our novel surface remeshing approach in the fourth and supplement it in the fifth section with both classical and real-life examples.

For the rest of the paper, we will assume that the surface Γ is given implicitly by the zero level set of some function $F\colon \Omega \subseteq \mathbb{R}^3 \to \mathbb{R}$, i. e.

$$\Gamma = \left\{ (x, y, z)^T \in \Omega \mid F(x, y, z) = 0 \right\}, \tag{1}$$

for some bounded domain Ω.

2. Higher Dimensional Embedding

In [19], the authors introduce the higher dimensional embedding technique which fits a a triangular surface mesh to a given geometry by enlarging the space we are originally interested in. The key assumption of HDE is that a uniform isotropic mesh in a higher-dimensional space will correspond to an anisotropic mesh in a lower-dimensional space.

This concept is best explained with Figure 2. The left image shows a uniform isotropic triangular mesh in $\mathbb{R}^3$. However, if projected onto $\mathbb{R}^2$ the mesh becomes anisotropic which is shown in the picture on the right.

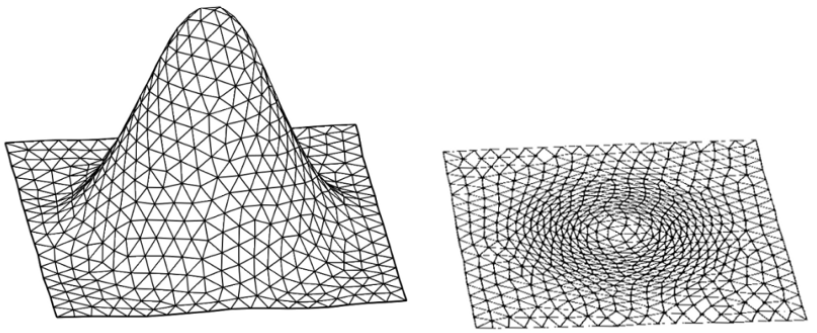

Fig. 2: An isotropic mesh in the higher-dimensional space $\mathbb{R}^3$ (left) and the corresponding anisotropic mesh in $\mathbb{R}^2$ (right). This picture encapsulates the key idea behind the higher dimensional embedding technique [19].

To obtain an anisotropic curvature-adapted mesh of an input surface $\Gamma \subset \mathbb{R}^3$, we define the embedding map $\Psi : \Gamma \to \mathbb{R}^6$ by

$$\Psi(\mathbf{x}) = (x,\, y,\, z,\, \sigma\, n_x,\, \sigma\, n_y,\, \sigma\, n_z)^T\,, \tag{2}$$

where $\mathbf{n} = (n_x, n_y, n_z)^T$ denotes the unit normal to Γ at $\mathbf{x} = (x,\, y,\, z)^T$ and $\sigma > 0$ is a constant that controls the influence of the normals in the embedding map. For small σ the mapping Ψ is close to the identity in $\mathbb{R}^3$ embedded in $\mathbb{R}^6$, i. e. $\Psi(\mathbf{x}) \approx (x, y, z, 0, 0, 0)^T$. Larger values of σ put more emphasis on the normal components of the surface Γ.

In the higher-dimensional space points on Γ are enriched with surface normal information. Consider for instance two generic points $\mathbf{a}, \mathbf{b} \in \Gamma$ and the edge $\overline{\mathbf{ab}}$. If the surface is flat, the normals at the endpoints are the same. Consequently, the length of the edge in $\mathbb{R}^3$, denoted with $l_{\mathbf{ab}}$, coincides exactly with the length measured in the higher-dimensional space $l^{6d}_{\mathbf{ab}}$. On the other hand, if the surface is curved, the normals at the endpoints are different and $l^{6d}_{\mathbf{ab}}$ becomes much larger than $l_{\mathbf{ab}}$.

2.1. Mesh Generation in Higher Dimensions

There are two established ways to build a uniform isotropic mesh in the higher-dimensional space. In [19], the authors propose an approach based on the Restricted Centroidal Voronoi Tessellation. In [4,6], a different method was proposed to construct a uniform isotropic mesh in the higher-dimensional space. The idea behind the latter method is to exploit the standard scalar product in the higher-dimensional space. Consider three points $\mathbf{a}$, $\mathbf{b}$ and $\mathbf{c}$ on the surface Γ, then the lengths and the angles in the higher-dimensional space are defined via

$$l^{6d}_{\mathbf{ab}} := \big\| \Psi(\mathbf{a}) - \Psi(\mathbf{b}) \big\|_{6\mathrm{d}} := \sqrt{\Big(\Psi(\mathbf{a}) - \Psi(\mathbf{b}), \Psi(\mathbf{a}) - \Psi(\mathbf{b})\Big)_{6\mathrm{d}}} \quad \text{and} \quad \cos\left(\theta^{6d}_{\mathbf{acb}}\right) := \frac{\Big(\Psi(\mathbf{a}) - \Psi(\mathbf{c}), \Psi(\mathbf{b}) - \Psi(\mathbf{c})\Big)_{6\mathrm{d}}}{l^{6d}_{\mathbf{ac}}\, l^{6d}_{\mathbf{bc}}}\,. \tag{3}$$

Now, one can fix a target edge length l^{6d} in the higher-dimensional space and modify an initial mesh Γ^{ini}_h in such a way that

$$l^{6d}_{\mathbf{e}} \approx l^{6d} \qquad \text{and} \qquad \cos\left(\theta^{6d}_{\alpha}\right) \approx \frac{1}{2} \qquad \forall \mathbf{e} \in \mathcal{E} \quad \text{and} \quad \forall \alpha \in \mathcal{A}\,, \tag{4}$$

where $\mathcal{E}$ and $\mathcal{A}$ are the sets of edges and angles of all mesh triangles.

Remark 2.1. *The method proposed in [4,6] does not embed the mesh in $\mathbb{R}^6$. Only the lengths and angles are computed in the higher-dimensional space. The mesh is modified in $\mathbb{R}^3$ by standard mesh operations for triangular elements such as edge flipping, edge splitting/contraction and node smoothing.*

3. Geometry Reconstruction with Radial Basis Functions

Radial basis functions are commonly divided into two categories: positive definite and conditionally positive definite functions. We state both definitions here.

Definition 3.1 (Positive definite function). *Let $\Phi\colon \mathbb{R}^d \to \mathbb{R}$ be a continuous function. We define the matrix $A_{\Phi,X}$ via its ij^{th} entry*

$$a_{ij} = \Phi(\mathbf{x}_i - \mathbf{x}_j)\,, \tag{5}$$

for any data set $X = \{\mathbf{x}_1, \dots, \mathbf{x}_N\} \subseteq \mathbb{R}^d$ of arbitary length $N \geq 1$. The function Φ is called positive definite *if the quadratic form*

$$\mathbf{c}^T A_{\Phi,X}\mathbf{c} \tag{6}$$

is positive for all vectors $\mathbf{c} \in \mathbb{R}^N \setminus \{\mathbf{0}\}$.

Definition 3.2 (Conditionally positive definite function). *Let $\mathcal{P}_m(\mathbb{R}^d)$ denote the space of d variate polynomials with absolute degree at most m and dimension $q := \dim \mathcal{P}_m(\mathbb{R}^d) = \binom{m-1+d}{d}$. For a basis $p_1, \dots, p_q$ of this space, define the $N \times q$ polynomial matrix P_X through its ij^{th} entry*

$$p_{ij} = p_i(\mathbf{x}_j)\,, \tag{7}$$

where $\mathbf{x}_j \in X$. The function Φ is called conditionally positive definite of order m *if the quadratic form* (6) *is positive for all X and for all $\mathbf{c} \in \mathbb{R}^N \setminus \{\mathbf{0}\}$ which additionally satisfy the constraint $P_X^T\mathbf{c} = \mathbf{0}$.*

One typically speaks of radial basis functions if one additionally assumes that Φ is a radial function, i.e. there exists a function $\phi\colon \mathbb{R}_{\geq 0} \to \mathbb{R}$ such that $\Phi(\mathbf{x}) = \phi(\|\mathbf{x}\|)$. Trivially, a positive definite function is also a conditionally positive definite function of order $m = 0$ and conditionally positive functions of order m are also conditionally positive for any order higher than m. Hence, the order usually shall denote the smallest positive integer m.

Suppose we want to recover a function $f\colon \mathbb{R}^d \to \mathbb{R}$ known on some data set $X = \{\mathbf{x}_i\}_{i=1}^N$. We can solve the interpolation problem

$$f(\mathbf{x}_i) = s(\mathbf{x}_i), \qquad 1 \leq i \leq N \tag{8}$$

for the interpolant $s\colon \mathbb{R}^d \to \mathbb{R}$ using radial basis functions by making the ansatz

$$s(\mathbf{x}) = \sum_{j=1}^{N} \alpha_j \Phi(\mathbf{x} - \mathbf{x}_j) \tag{9}$$

in the case of a positive definite Φ and

$$s(\mathbf{x}) = \sum_{j=1}^{N} \alpha_j \Phi(\mathbf{x} - \mathbf{x}_j) + \sum_{k=1}^{q} \beta_k p_k(\mathbf{x}) \tag{10}$$

in the case of conditionally positive definite functions. The coefficients $\boldsymbol{\alpha} = (\alpha_j) \in \mathbb{R}^N, \boldsymbol{\beta} = (\beta_k) \in \mathbb{R}^q$ need to be determined by applying the interpolation condition (8) to either (9) or (10). Hence one needs to solve either

$$A_{\Phi,X}\boldsymbol{\alpha} = \mathbf{f} \qquad \text{or} \qquad \begin{pmatrix} A_{\Phi,X} & P_X \\ P_X^T & 0 \end{pmatrix}\begin{pmatrix} \boldsymbol{\alpha} \\ \boldsymbol{\beta} \end{pmatrix} = \begin{pmatrix} \mathbf{f} \\ \mathbf{0} \end{pmatrix}, \tag{11}$$

where $\mathbf{f} = (f(\mathbf{x}_j))$.

For positive definite functions, the linear system is positive definite by construction. Hence the coefficients can be determined uniquely. It is also not difficult to verify that the second choice for an interpolant leads to unique coefficients in the case of conditionally positive definite functions, see [24, Theorem 8.21] for details. In the case of conditionally positive definite functions the Courant-Fischer theorem guarantees that at least $N - q$ eigenvalues of the matrix $A_{\Phi,X}$ are positive.

Another criterion to classify RBFs is whether they have compact support or not. This is an advantageous feature for very large data sets since the matrix $A_{\Phi,X}$ becomes sparse if the support radius is small enough. It is well known that for compactly supported RBFs the polynomial part in (10) has to vanish. There are no nontrivial conditionally positive definite functions with compact support [24, Theorem 9.1]. Wendland [23] presented a class of compactly supported radial basis functions which consist of polynomials within their support. The degree of the polynomials for a given space dimension and smoothness parameter is minimal. Compactly supported RBFs lead to sparse matrices $A_{\Phi,X}$ which implies that the condition behave better than for globally supported ones. A deeper analysis of these relationships are given in [3,24].

Common examples of RBFs are shown in Table 1.

Global support		Compact support ($d = 3$)	
e^{-r^2}	Gaussian	$\phi_{3,1}(r) = (1-r)_+^4(4r+1)$	C_2
$\sqrt{1+r^2}$	Multiquadric	$\phi_{3,2}(r) = (1-r)_+^6(35r^2+18r+3)$	C_4
$1/\sqrt{1+r^2}$	Inverse Multiquadric	$\phi_{3,3}(r) = (1-r)_+^8(32r^3+25r^2+8r+1)$	C_6
r^3	Polyharmonic Spline	due to Wendland [23]	

Table 1: Common examples of globally and compactly supported RBFs. All functions are positive definite except the polyharmonic spline which is conditionally positive definite for $d = 3$ with (minimal) order 2. For positive r the truncation operator $(\cdot)_+$ leaves its argument unaltered. For negative arguments it is set to zero. The last row indicates the regularity of the Wendland RBFs.

3.1. Surface reconstruction with RBFs

We cannot simply replace the target function f in (8) with the function F whose zero level set describes the implicit surface (1) since the right hand sides of the linear systems (11) vanish which implies that the coefficients vanish as well. Carr et al. [2] therefore made the additional assumption that the normal vectors are known. One then can also prescribe on-surface and off-surface points. Assume that the points on the surface are denoted with $X = \{\mathbf{x}_1, \dots, \mathbf{x}_N\}$ and the corresponding normal vectors with $M = \{\mathbf{n}_1, \dots, \mathbf{n}_N\}$. Then one can define the surface interpolation problem

$$\begin{aligned} s(\mathbf{x}_i) = F(\mathbf{x}_i) &= 0, && 1 \le i \le N && \text{(on-surface points)} \\ s(\mathbf{x}_i + \varepsilon\mathbf{n}_i) = F(\mathbf{x}_i + \varepsilon\mathbf{n}_i) &= \varepsilon, && N+1 \le i \le 2N && \text{(off-surface points)} \end{aligned} \tag{12}$$

for some parameter $\varepsilon > 0$. Since the right hand side is no longer zero, we find now nontrivial solutions to the linear systems (11). Actually, it is enough to define just one off-set point to get a nontrivial solution. Moreover it is even possible to add more constraints. One possibility is to consider $s(\mathbf{x}_i - \varepsilon\mathbf{n}_i) = F(\mathbf{x}_i - \varepsilon\mathbf{n}_i) = -\varepsilon$ for $2N + 1 \le i \le 3N$.

To reduce the computational cost when solving the linear system (11) or when projecting points onto the surface, we consider a partition as done in [3]. We denote the number of the patches in the partition by K. These patches may overlap and the magnitude of the overlap is given by the parameter Ov.

4. A Novel Anisotropic Surface Remeshing Approach

In this section, we describe the novel anisotropic curvature adapted remeshing procedure. More details can be found in [3]. Starting from a conformal triangular surface mesh Γ_h^{ini}, we proceed as follows:

(1) Build RBF approximation Γ_0^s of the initial surface mesh Γ_h^{ini} and

(2) Construct final adapted mesh Γ_h^{fin} via HDE including:

- several local mesh modifications and
- projections onto the surface Γ_0^s

In the following three paragraphs we describe the different parts of the remeshing procedure. More details can be found in [3].

Approximation of Γ_0^s. When constructing the continuous approximation of Γ_h^{ini}, the user has to specify the type of radial basis function Φ, the parameter ε, the number of partitions K and the overlap parameter Ov. In order to setup the interpolation problem defined in (12), we use the vertices of Γ_h^{ini} as interpolation nodes X. By averaging the normals of the triangles that share a generic vertex $\mathbf{x}_i$, we define the normals $\mathbf{n}_i$ at this point and obtain the set M. Finally, we construct and solve the linear system (11) to derive the continuous interpolant s. The whole procedure to build the function s whose zero level set is the smooth surface Γ_0^s is described in Algorithm 1

Algorithm 1 The construction of the function s whose zero level set is the smooth surface Γ_0^s.

surfaceApproximation($\Gamma_h^{ini}, \Phi, \varepsilon, K, Ov$)

1: compute normals $\mathbf{n}_i$
2: define the set $X = \{\mathbf{x}_1, \mathbf{x}_2, \ldots, \mathbf{x}_N, (\mathbf{x}_1 + \varepsilon\mathbf{n}_1), (\mathbf{x}_2 + \varepsilon\mathbf{n}_2), \ldots, (\mathbf{x}_N + \varepsilon\mathbf{n}_N)\}$
3: compute the matrix $A_{\Phi,X}$, see (5)
4: **if** Φ is conditionally positive **then**
5: compute the matrix P_X, see (7)
6: **end if**
7: set the r.h.s. $\mathbf{f}(i) = 0$ if $i \leq N$ otherwise $\mathbf{f}(i) = \varepsilon$
8: solve the linear system (11)

Local Mesh Modifications. Next, we modify Γ_h^{ini} so that it becomes a uniform isotropic mesh in the higher-dimensional space. To achieve this goal two inputs are required: the parameter σ, appearing in the embedding map Ψ, as well as the target length in the higher-dimensional space l^{6d}. We consider the adaptation scheme proposed in [3,4,6] to get a uniform isotropic mesh in the higher dimensional space. In Algorithm 2 we report the pseudo-code of this adaptation procedure which This adaptation procedure exploits all standard mesh modifications such as edge flipping, edge splitting/contraction and node smoothing.

Algorithm 2 The anisotropic mesh adaptation.

meshAdaptation(Γ_h^{ini}, `maxIter`)

1: **for** $i \in \{1, ..., \texttt{maxIter}\}$ **do**
2: **repeat**
3: contract the edges $l_{\mathbf{e}}^{6d} < 0.5\, l^{6d}$
4: smooth 30% of vertices
5: edge flips improvement
6: **until** an edge $\mathbf{e}$ is contracted
7: split the edges $l_{\mathbf{e}}^{6d} > 1.5\, l^{6d}$
8: edge flips improvement
9: smooth 30% of vertices
10: edge flips improvement
11: **end for**

Projection of nodes onto Γ_0^s. Applying standard mesh operations naively will fail. Consider, for instance, the edge splitting operation. If we simply halve the edge, the new point lies only under very special circumstances on Γ_0^s. Moreover, since the new point is usually not on the surface, the unit normal is not defined. Node smoothing leads to a similar problem. To avoid this issue, we exploit a projection algorithm. If we split an edge or move a point using node

smoothing, we project the resulting point onto the reconstructed surface [17]. Then, we define the normal of the newly added point via the gradient of the surface interpolant [3].

The edge contraction has a similar issue since the edge can be contracted to different locations. Therefore, we contract it to one of the endpoints [7] to avoid having to project this point onto Γ_0^s. In fact, the endpoints lie on Γ_0^s by construction and the normals at these points are well-defined. Figure 3 provides a two-dimensional example.

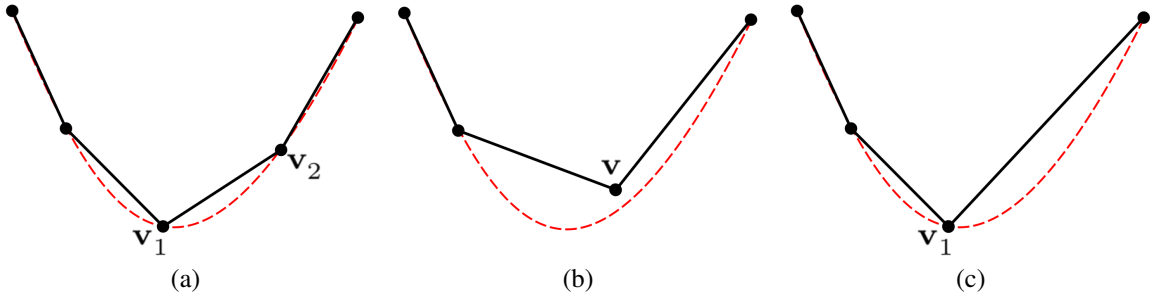

Fig. 3: Figure (a) shows a fine input mesh (solid line) which approximates the reconstructed curve (dashed line). In Figure (b), the edge $\overline{\mathbf{v}_1\mathbf{v}_2}$ is contracted to its midpoint $\mathbf{v}$, which does not lie on the reconstructed curve. However, in Figure (c) the edge $\overline{\mathbf{v}_1\mathbf{v}_2}$ in contracted to the end point $\mathbf{v}_1$ which by construction automatically lies on the dashed curve.

5. Numerical Examples

In the following, we study different input meshes. We will show that our method can not only be used to fill in more detail but also to thin out out very complex meshes. Finally, we apply our method to a mesh coming from a medical application.

To assess the degree of anisotropy of our mesh, we compute the *global aspect ratio*

$$q_{\Gamma_h} := \max_{T \in \Gamma_h} q_T \,, \tag{13}$$

where $q_T := R_T/(2\, r_T)$ is the so called *aspect ratio* of the triangle T. Here R_T and r_T are the radii of the circumscribed and inscribed circle of T, respectively [21]. We observe that $q_T \geq 1$ by construction. If $q_T = 1$, then T is an equilateral triangle, while if $q_T \gg 1$, the triangle T is stretched.

A sensitivity analysis for the parameters Ov, l^{6d} and σ is provided in [3].

5.1. Bunny

We examine the well-known Stanford bunny, depicted in Figure 4. To construct Γ_0^s, we use thin plate splines, $\varepsilon = 0.001$, $K = 200$, $Ov = 3$. We run the anisotropic adaptation procedure with $l^{6d} = 0.001$ and $\sigma = 1.0$. In Figure 4, we show both the initial and the resulting mesh. The resulting mesh is strongly anisotropic, in fact the global aspect ratio q_{Γ_h} is $3.989e{+}02$ and it is more refined than the initial one. While the initial mesh has 69 451 elements, the final one has 110 350 triangles.

The triangles are aligned and stretched according to the curvature of the surface. This can be clearly seen when zooming in on the ears of the bunny, see Figures 5. In the initial mesh Γ_h^{ini}, the triangles are too big to capture the helix of the bunny's ears and their orientation and shape do not reflect the curvature of the surface. However in the final mesh Γ_h^{fin} all these features disappear.

Moreover, the final anisotropic adapted mesh makes details in the mesh more apparent. For instance, unlike for the initial mesh Figure 4 (left), finer details in the fur of the bunny are clearly visible in the final mesh, see Figure 4 (right).

5.2. Lucy

Our anisotropic mesh adaptation procedure can be used to simplify a dense initial mesh by coarsening it in regions with little curvature variation. We consider the geometry shown in Figure 6. This mesh is another well-known

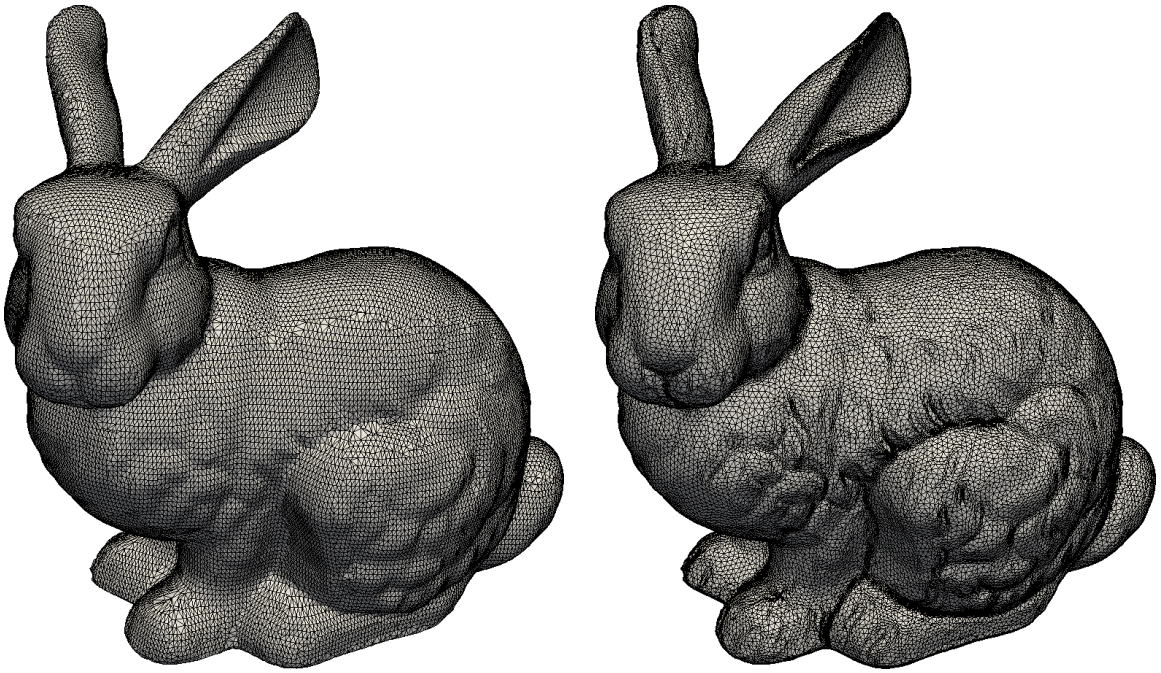

Fig. 4: The initial bunny mesh (left) and the resulting anisotropic adapted one (right).

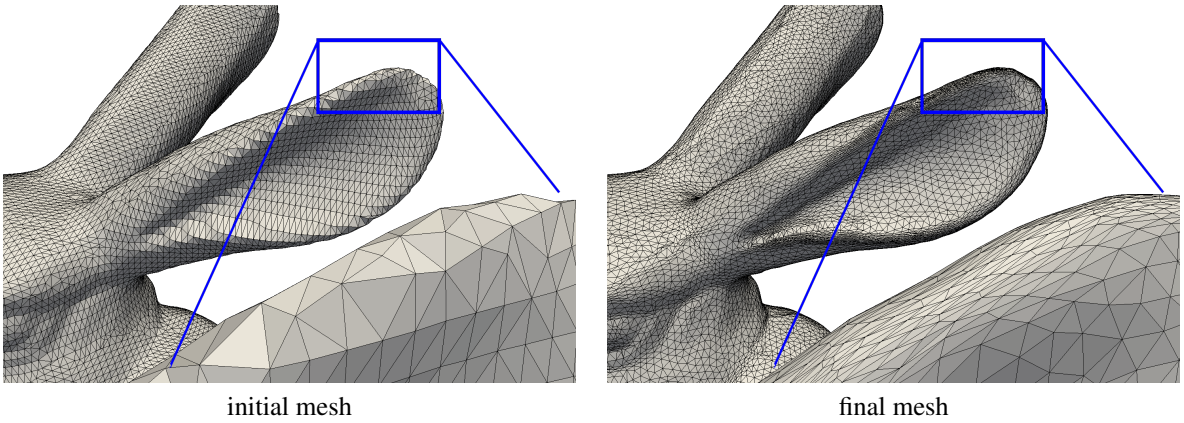

Fig. 5: A detail of the initial bunny mesh (left) and the same detail for the anisotropic adapted one (right).

benchmark in surface mesh adaptation ("Lucy"). Here the mesh is so fine that one would not be able to see the faces of the triangles because of the density of the edges, see Figure 6 left. Hence we only show the faces of the surface without the edges. To construct the surface approximation, we use thin plate splines, $\varepsilon = 0.1$, $K = 3000$, $Ov = 3$ and the $\sigma = 10$. We point out that the number of partitions is rather high. If we want to reduce the number of partitions or avoid dealing with large dense linear systems, we can employ compactly supported RBFs.

The initial mesh offers a very fine approximation of the input geometry, but managing this huge data set requires an unacceptably high computational effort. By choosing a large target length l^{6d} our anisotropic adaptation procedure effectively becomes a mesh simplification method. The details in Figure 7 show that the shape of the initial mesh is still preserved, however, using considerably fewer elements. To be more precise, we reduce the number of elements by 73%

for $l^{6d} = 30$ and by 87% for $l^{6d} = 50$. The final meshes are more anisotropic compared to the initial one. We increase the global aspect ratio q_{Γ_h} from 1.21 to 95.83 and to 65.04, for $l^{6d} = 30$ and $l^{6d} = 50$, respectively.

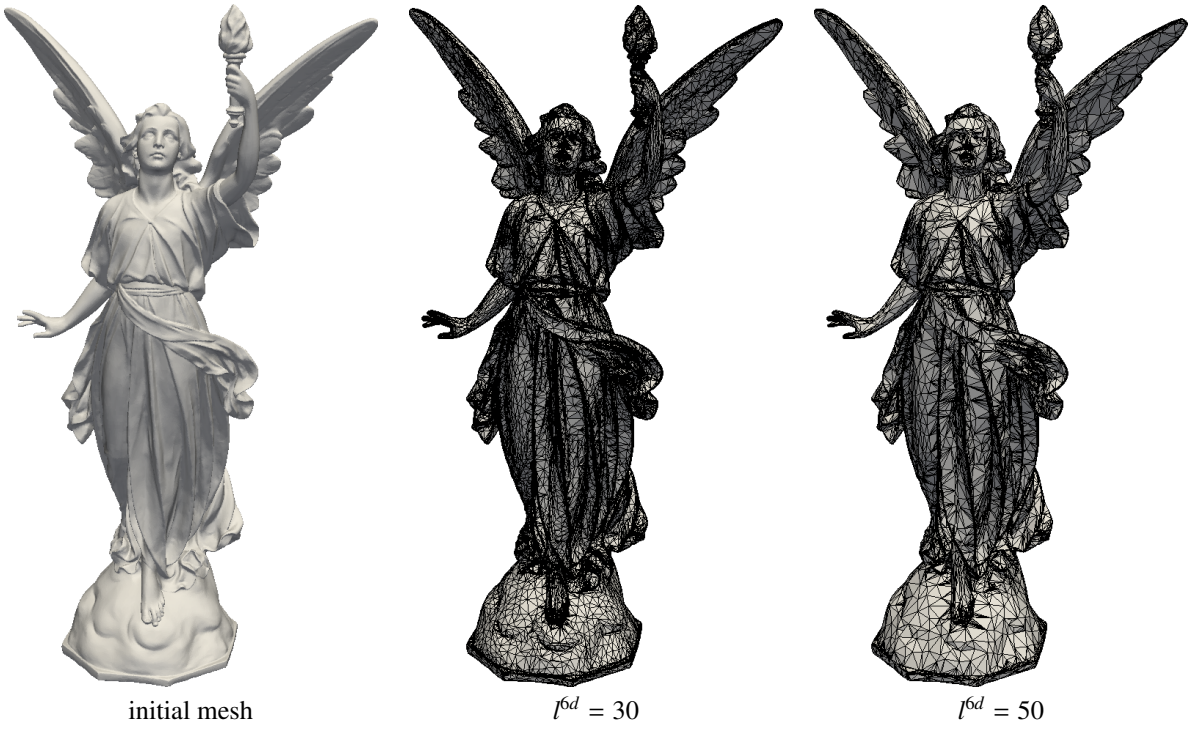

Fig. 6: The "Lucy" mesh with 510 180 elements (without edges) as well as the thinned out meshes for $l^{6d} = 30$ and 141 674 elements as well as for $l^{6d} = 50$ and 67 888 elements.

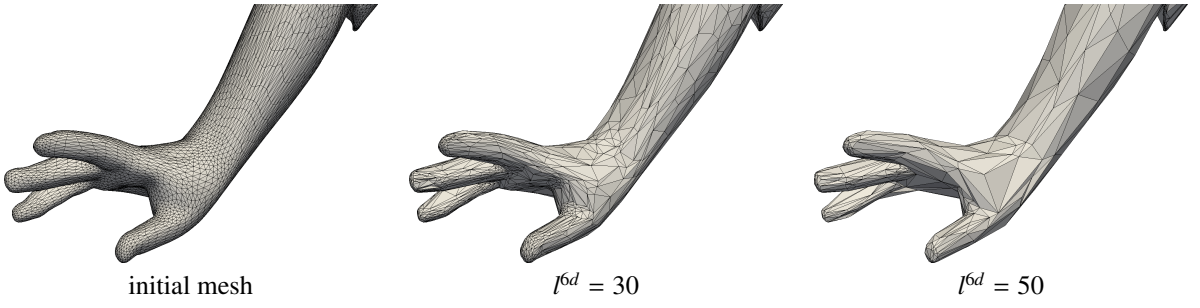

Fig. 7: A detail of the "Lucy" mesh which is thinned out according to different target edge lengths.

5.3. Real-life Example: Bronchus

Finally, we discuss a mesh of the trachea and the main branches of the bronchi [11]. The geometry is rather complex. It consists of a sequences of branches that become smaller at each bifurcation. Triangles in the initial mesh are not aligned according to the curvature of the geometry, see Figure 9.

The surface Γ_0^s is built using thin plate splines, $\varepsilon = 0.1$, $K = 200$, $Ov = 3$. We set σ to 1 and consider three different target edge lengths

$$l^{6d} \in \{0.25,\ 0.5,\ 1.0\}\,.$$

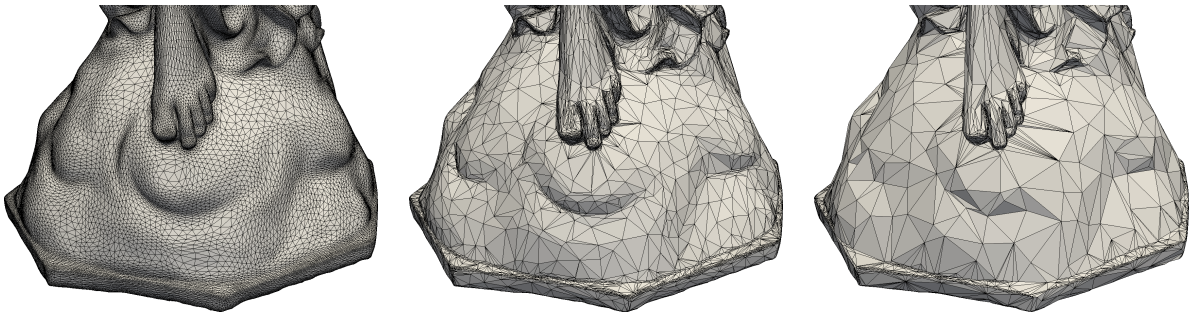

Fig. 8: A detail of the "Lucy" mesh which is thinned out according to different target edge lengths.

After applying our remeshing procedure the previously problematic triangles disappear and are replaced by new curvature-aligned ones. This example underlines the flexibility of the proposed adaptation procedure. In fact, it is possible to achieve different tasks by tuning the parameter l^{6d}. On the one hand, if we consider a large value for l^{6d}, the remeshing process becomes a mesh simplification method, see the detail in Figure 9 corresponding to $l^{6d} = 1.0$. On the other hand, if we consider a relatively short target edge length, our algorithm creates a surface mesh that is smoother and finer than the initial one, see the detail in Figure 9 corresponding to $l^{6d} = 0.25$. Moreover, if we tune the target length in such a way that we obtain approximately the same amount of elements as in Γ_h^{ini}, the computational effort to deal with this mesh is the same as before but its triangles are curvature-aligned. See Figure 9 with target edge length $l^{6d} = 0.5$.

This observation is numerically verified by the data in Table 2. Here we state the number of elements in the initial and adapted meshes for different target lengths. In this table, we additionally provide the values of the global aspect ratio q_{Γ_h} which quantify the degree of anisotropy.

	initial mesh	$l^{6d} = 0.5$	$l^{6d} = 1.0$	$l^{6d} = 0.25$
#ele	42 692 100%	34 954 82%	12 026 28%	132 784 311%
q_{Γ_h}	6.00e+01	1.28e+02	7.53e+02	7.08e+02

Table 2: The number of elements for the bronchus meshes. We provide the percentage of the triangles in the mesh with respect to the number of triangles in the adapted meshes as well as the global aspect ratios.

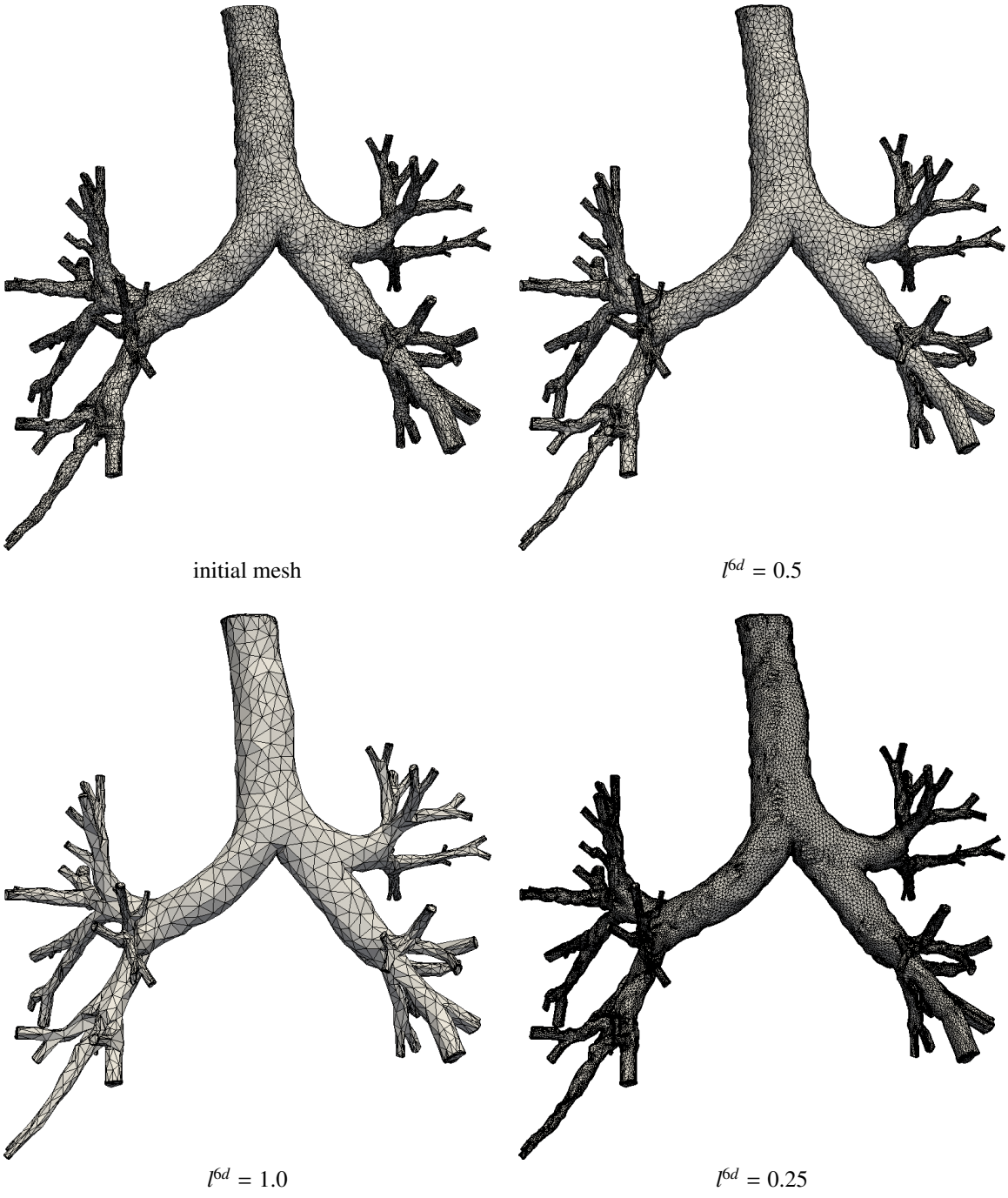

Fig. 9: The initial bronchus mesh, courtesy Fetita *et al.* [11], and the adapted ones for different target edge lengths.

6. Conclusion

We presented a new anisotropic surface remeshing algorithm, which can be used to improve problematic inputs coming from discrete surface data sets. The anisotropy is guided by the curvature of the surface. Depending on the target edge length parameter, our new method becomes either a mesh simplification, a surface remeshing or a fill-in

algorithm. In particular, when the initial mesh is extremely coarse, the algorithm increases the resolution of the poor initial data. At the moment our method will smooth sharp edges and corners. Future research will need to be conducted to study how to circumvent this problem.

Acknowledgments. The work of Franco Dassi was partially supported under the "Leibniz - DAAD Research Fellowship 2014".

References

[1] G. D. Cañas and S. J. Gortler, *Surface remeshing in arbitrary codimensions*, Vis. Comput., 22 (2006), pp. 885–895.

[2] J. C. Carr, R. K. Beatson, J. B. Cherrie, T. J. Mitchell, W. R. Fright, B. C. McCallum, and T. R. Evans, *Reconstruction and representation of 3d objects with radial basis functions*, in Proceedings of the 28th annual conference on Computer graphics and interactive techniques, ACM, 2001, pp. 67–76.

[3] F. Dassi, P. Farrell, and S. Hang, *A novel surface remeshing scheme via higher dimentsional embedding and radial basis functions*, Tech. Report 2265, WIAS, Berlin, 2016.

[4] F. Dassi, A. Mola, and H. Si, *Curvature-adapted remeshing of CAD surfaces*, Procedia Engineering, 82 (2014), pp. 253 – 265, doi:http://dx.doi.org/10.1016/j.proeng.2014.10.388, http://www.sciencedirect.com/science/article/pii/S1877705814016671. 23rd International Meshing Roundtable (IMR23).

[5] F. Dassi, S. Perotto, L. Formaggia, and P. Ruffo, *Efficient geometric reconstruction of complex geological structures*, Mathematics and Computers in Simulation, 106 (2014), pp. 163 – 184, doi:http://dx.doi.org/10.1016/j.matcom.2014.01.005, http://www.sciencedirect.com/science/article/pii/S0378475414000184.

[6] F. Dassi and H. Si, *New Challenges in Grid Generation and Adaptivity for Scientific Computing*, Springer International Publishing, Cham, 2015, ch. A Curvature-Adapted Anisotropic Surface Re-meshing Method, pp. 19–41, doi:10.1007/978-3-319-06053-8_2, http://dx.doi.org/10.1007/978-3-319-06053-8_2.

[7] H. Edelsbrunner, *Geometry and topology for mesh generation*, Cambridge University Press, 2001.

[8] J. Escobar, G. Montero, R. Montenegro, and E. Rodríguez, *An algebraic method for smoothing surface triangulations on a local parametric space*, International Journal for Numerical Methods in Engineering, 66 (2006), pp. 740–760.

[9] P. Farrell and H. Wendland, *RBF Multiscale Collocation for Second Order Elliptic Boundary Value Problems*, SIAM J. Numer. Anal., 51 (2013), pp. 2403–2425.

[10] G. E. Fasshauer, *Meshfree Approximation Methods with MATLAB*, vol. 6 of Interdisciplinary Mathematical Sciences, World Scientific Publishing, Hackensack, 2007.

[11] C. Fetita, S. Mancini, D. Perchet, F. Preteux, M. Thirie, and L. Vial, *An image-based computational model of oscillatory flow in the proximal part of tracheobronchial trees*, Comput. Methods Biomech. Biomed. Engin., 8 (2005), pp. 279 – 293.

[12] L. Formaggia, S. Micheletti, and S. Perotto, *Anisotropic mesh adaptation in computational fluid dynamics: Application to the advection-diffusion-reaction and the Stokes problems*, Appl. Numer. Math., 51 (2004), pp. 511–533, doi:10.1016/j.apnum.2004.06.007, http://dx.doi.org/10.1016/j.apnum.2004.06.007.

[13] L. Formaggia and S. Perotto, *New anisotropic a priori error estimates*, Numer. Math., 89 (2001), pp. 641–667.

[14] P. J. Frey, *Generation and adaptation of computational surface meshes from discrete anatomical data*, International Journal for Numerical Methods in Engineering, 60 (2004), pp. 1049–1074.

[15] P. J. Frey and F. Alauzet, *Anisotropic mesh adaptation for CFD computations*, Comput. Meth. Appl. Mech. Engrg., 194 (2005), pp. 5068–5082.

[16] P. J. Frey and H. Borouchaki, *Geometric surface mesh optimization*, Comput. Vis. Sci., 1 (1998), pp. 113–121.

[17] E. Hartmann, *On the curvature of curves and surfaces defined by normalforms*, Computer Aided Geometric Design, 16 (1999), pp. 355 – 376, doi:http://dx.doi.org/10.1016/S0167-8396(99)00003-5, http://www.sciencedirect.com/science/article/pii/S0167839699000035.

[18] A. Iske, *Multiresolution Methods in Scattered Data Modelling*, vol. 37 of Lecture Notes in Computational Science and Engineering, Springer, Berlin, 2004.

[19] B. Lévy and N. Bonneel, *Variational anisotropic surface meshing with voronoi parallel linear enumeration*, in Proceedings of the 21st International Meshing Roundtable, Springer, 2013, pp. 349–366.

[20] E. Marchandise, C. Piret, and J.-F. Remacle, *Cad and mesh repair with radial basis functions*, Journal of Computational Physics, 231 (2012), pp. 2376 – 2387, doi:http://dx.doi.org/10.1016/j.jcp.2011.11.033, http://www.sciencedirect.com/science/article/pii/S0021999111006899.

[21] J. R. Shewchuk, *What is a good linear finite element? - interpolation, conditioning, anisotropy, and quality measures*, tech. report, In Proc. of the 11th International Meshing Roundtable, 2002.

[22] V. Surazhsky and C. Gotsman, *Explicit surface remeshing*, in Proceedings of the 2003 Eurographics/ACM SIGGRAPH symposium on Geometry processing, Eurographics Association, 2003, pp. 20–30.

[23] H. Wendland, *Piecewise Polynomial, Positive Definite and Compactly Supported Radial Functions of Minimal Degree*, Adv. Comput. Math., 4 (1995), pp. 389–396, doi:10.1007/BF02123482, http://dx.doi.org/10.1007/BF02123482.

[24] H. Wendland, *Scattered Data Approximation*, vol. 17 of Cambridge Monographs on Applied and Computational Mathematics, Cambridge University Press, Cambridge, 2005.